



ELSEVIER

Available online at www.sciencedirect.com

SCIENCE @ DIRECT®

Earth and Planetary Science Letters 213 (2003) 15–30

EPSL

www.elsevier.com/locate/epsl

New insights into Archean sulfur cycle from mass-independent sulfur isotope records from the Hamersley Basin, Australia

Shuhei Ono^{a,*}, Jennifer L. Eigenbrode^b, Alexander A. Pavlov^c,
Pushker Kharecha^b, Douglas Rumble III^a, James F. Kasting^b,
Katherine H. Freeman^b

^a *Geophysical Laboratory, Carnegie Institution of Washington, 5251 Broad Branch Rd., Washington, DC 20015, USA*

^b *Astrobiology Research Center, the Pennsylvania State University, University Park, PA 16802, USA*

^c *LASPI/University of Colorado, Duane Physics Building, 392 UCB, Boulder, CO 80309, USA*

Received 10 January 2003; received in revised form 9 May 2003; accepted 9 May 2003

Abstract

We have measured multiple sulfur isotope ratios ($^{34}\text{S}/^{33}\text{S}/^{32}\text{S}$) for sulfide sulfur in shale and carbonate lithofacies from the Hamersley Basin, Western Australia. The $\Delta^{33}\text{S}$ values ($\Delta^{33}\text{S} \approx \delta^{33}\text{S} - 0.515 \times \delta^{34}\text{S}$) shift from -1.9 to $+6.9\text{‰}$ over a 22-m core section of the lower Mount McRae Shale (~ 2.5 Ga). Likewise, sulfide sulfur analyses of the Jeerinah Formation (~ 2.7 Ga) yield $\Delta^{33}\text{S}$ values of -0.1 to $+8.1\text{‰}$ over a 50-m section of core. Despite wide variations in $\Delta^{33}\text{S}$ and $\delta^{34}\text{S}$, these two shale units yield a similar positive correlation between $\Delta^{33}\text{S}$ and $\delta^{34}\text{S}$. In contrast, pyrite sulfur analyses of the Carawine Dolomite (~ 2.6 Ga) yield a broad range in $\delta^{34}\text{S}$ ($+3.2$ to $+16.2\text{‰}$) but a relatively small variation and negative values in $\Delta^{33}\text{S}$ (-2.5 to -1.1‰). The stratigraphic distribution of $\delta^{33}\text{S}$, $\delta^{34}\text{S}$, and $\Delta^{33}\text{S}$ in Western Australia allows us to speculate on the sulfur isotopic composition of Archean sulfur reservoirs and to trace pathways in the Archean sulfur cycle. Our data are explained by a combination of mass-independent fractionation (MIF) in the atmosphere and biological mass-dependent fractionation in the ocean. In the Archean, volcanic, sulfur-bearing gas species were photolysed by solar ultraviolet (UV) radiation in an oxygen-free atmosphere, resulting in MIF of sulfur isotopes. Aerosols of S_8 (with $\Delta^{33}\text{S} > 0$) and sulfuric acid (with $\Delta^{33}\text{S} < 0$) formed from the products of UV photolysis and carried mass-independently fractionated sulfur into the hydrosphere. The signatures of atmospheric photolysis were preserved by precipitation of pyrite in sediments. Pyrite precipitation was mediated by microbial enzymatic catalysis that superimposed mass-dependent fractionation on mass-independent atmospheric effects. Multiple sulfur isotope analyses provide new insights into the early evolution of the atmosphere and the evolution and distribution of early sulfur-metabolizing organisms.

© 2003 Elsevier Science B.V. All rights reserved.

Keywords: mass-independent fractionation; S-33; sulfur isotope; Archean; Hamersley Basin; atmospheric evolution; sulfur cycle

* Corresponding author. Tel.: +1 202-478-8988; Fax: +1 202-478-8901.

E-mail address: s.ono@gl.ciw.edu (S. Ono).

1. Introduction

Mass-independent fractionation (MIF) is a term describing an unconventional relationship between two isotope ratios that violates the mass-dependent rule (e.g. $\delta^{17}\text{O} \approx 0.516 \times \delta^{18}\text{O}$, $\delta^{33}\text{S} \approx 0.515 \times \delta^{34}\text{S}$) [1,2]. A capital delta notation is used to express the degree of MIF. The MIF in ^{33}S is defined as $\Delta^{33}\text{S} \approx \delta^{33}\text{S} - 0.515 \times \delta^{34}\text{S}$, which is a deviation of the measured value of $\delta^{33}\text{S}$ from that expected from $\delta^{34}\text{S}$. Formulas using exponential or logarithmic terms are used for more accurate calculation of $\Delta^{33}\text{S}$ [2–4]. A theoretical explanation for the origin of MIF is currently under development [5]. Experiments show, however, that ultraviolet (UV) photolysis of gas molecules produces MIF effects in oxygen and sulfur isotope systems [1,2,6].

The discovery of sulfur isotope MIF in Archean sulfide and sulfate minerals raised hopes that a quantitative, time-resolved history of the oxygenation of Earth's atmosphere during the Paleoproterozoic was at last in hand [2]. The discovery of the Archean sulfur MIF was subsequently confirmed by two other laboratories, one using laser fluorination mass spectrometry [7–10] and the other using secondary ion mass spectrometry [11,12]. According to the discoverers' model, the sulfur MIF signature in Archean rocks was caused by photochemical reactions of volcanic sulfur species induced by solar UV radiation in an atmosphere devoid of an ozone shield [2,13]. The absence of sulfur MIF signatures in rocks younger than 2.0 Ga was correlated with an increase in atmospheric oxygen levels to higher than 10^{-2} times the present atmospheric level (PAL) and the establishment of an ozone shield blocking UV radiation [2,13]. If this hypothesis is correct, a chronologic oxygenation history would be available in sulfide- or sulfate-bearing rock samples spaced across an early Proterozoic stratigraphic interval.

Today, sulfur enters the atmosphere through volcanic outgassing of SO_2 and H_2S and from a variety of biological (including anthropogenic) sources. Reduced sulfur gases are oxidized to either SO_2 or H_2SO_4 (sulfuric acid), which is removed from the atmosphere by rainout or wet

deposition. Ultimately, all sulfur becomes fully oxidized and part of the oceanic dissolved sulfate reservoir. Thus, any MIF signature that might have been produced by photochemical reactions is erased when the different sulfur species become homogenized [14,15]. The difficulty of preserving mass-independently fractionated sulfur isotopes in an oxygenated atmosphere is emphasized by the recent discovery of small isotope anomalies in atmospheric aerosols [16]. Values of $\Delta^{33}\text{S}$ in aerosol particles collected directly from the atmosphere range from +0.1 to +0.5‰. Oxygen MIF anomalies, however, are preserved more easily in the modern atmosphere with sulfate aerosol $\Delta^{17}\text{O}$ anomalies of +0.9 to +3.2‰ [17]. The geologic record of MIF anomalies in polar ice cores shows that sulfur anomalies ($\Delta^{33}\text{S} = -0.5$ to +0.7‰) are associated with giant volcanic eruptions such as Mt. Pinatubo (June 15, 1991) whose eruptive clouds penetrate deeply into the stratosphere [18]. Through photochemical modeling, Pavlov and Kasting [15] found that difficulties in preserving sulfur MIF extend to O_2 levels as low as 10^{-5} PAL. Thus, the upper limit on $p\text{O}_2$ in the pre-2.3 Ga atmosphere is even lower than deduced by Farquhar et al. [13].

Here, we report the first stratigraphically resolved analyses of multiple sulfur isotope ratios ($^{34}\text{S}/^{33}\text{S}/^{32}\text{S}$) of well-preserved sedimentary rocks from the late Archean Hamersley Province, Western Australia. Our new analyses expand the entire known natural range of variation in sulfur isotope MIF anomalies [2,11] by a factor of three. While these measurements fully support the existence of MIF in sulfur isotopes in Archean rocks, the systematic relationships between $\delta^{33}\text{S}$ and $\delta^{34}\text{S}$ in our measurements permit further speculation on the isotopic composition of Archean sulfur reservoirs and give some new insights into how isotopic signatures of atmospheric photochemistry could have been produced, transported and preserved in the Archean sediments.

2. Geology

The Hamersley Basin, Western Australia, comprises a rare and well-preserved supracrustal suc-

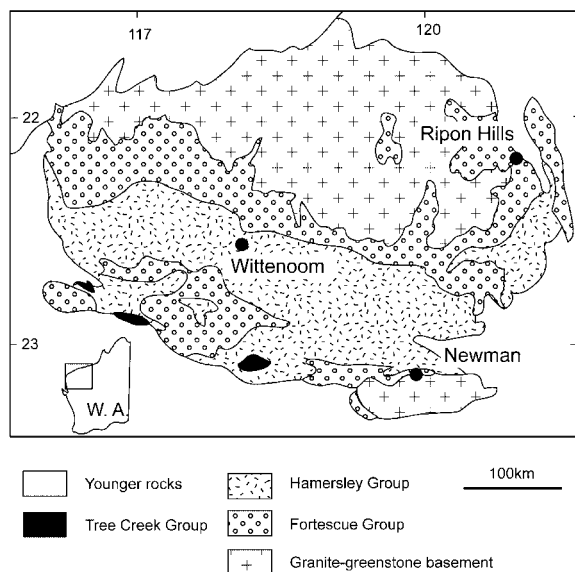


Fig. 1. Geological map of the Hamersley Basin and the location of core samples used for this study.

cession of volcanic and sedimentary rocks that were deposited between 2.77 Ga and 2.41 Ga on the granitoid-greenstone terrain referred to as the Pilbara Craton [19–22] (Fig. 1). Across the basin, this succession has been subjected to sub-green-schist facies burial metamorphism [23] and, locally, subjected to hydrothermal alteration giving rise to the prominent ore deposits of the region.

The Mount Bruce Supergroup (or Mt. Bruce Megasequence Set by [21]) covers an area of over 90 000 km² and is broken down into three groups: the Turee Creek Group, the Hamersley Group and the Fortescue Group [19–21]. This study focuses on the Jeerinah Formation of the Fortescue Group and the Carawine Dolomite and the Mount McRae Shale of the Hamersley Group. The Jeerinah Formation is a deep-water marine succession dominated by carbonaceous pyritic shales that, in the central region, gradually passes upward into the Marra Mamba Iron Formation and the Wittenoom Formation [19,22]. Iron formation is absent in the east where the Jeerinah Formation (formerly referred to the Lewin Shale in this region) is conformably overlain by the Carawine Dolomite, a carbonate platform deposit with carbonate turbidites at its base and shallow-water stromatolitic carbonates at its

top [24]. SHRIMP U–Pb zircon dates for the base and top of the Jeerinah Formation in the central region are 2684 ± 6 Ma [20] and 2629 ± 5 Ma [25], respectively. The age of the Carawine Dolomite is not yet constrained by SHRIMP U–Pb dates. Its correlation to the central succession is unclear. The Mt. McRae Shale is marine shale conformably underlain by the Mount Sylvia Shale and overlain by the Brockman Iron Formation. It is composed of carbonaceous pyritic shale and minor chert [19,26]. The age of the Mt. McRae Shale is bracketed by U–Pb zircon ages of 2561 ± 8 Ma for the Wittenoom crystal-rich tuff below [27] and 2479 ± 3 for the S9 band of the Brockman Iron Formation above [25].

3. Materials

The samples used in this study came from three drill cores: Aus No. 493 drilled near the Mt. Whaleback Mine in the Mt. Newman Area [28]; WRL1 drilled near Wittenoom ($22^{\circ}11.7'S$, $118^{\circ}12.6'E$); and RHDH2a drilled near the Ripon Hills ($21^{\circ}17'E$, $120^{\circ}50'S$). The locations of the samples are shown in Fig. 1.

Fifteen samples were collected from a 22-m section of Aus No. 493 core, which represents the lower part of the Mt. McRae Shale. The same drill core was studied by Kakegawa et al. [28], who used a laser oxidation system to determine $\delta^{34}S$ from 100- μ m diameter spots on rock chips. A range in $\delta^{34}S$ from -6.3 to $+11.8$ ‰ was reported from the core [28]. In the upper part of the core section (< 8 m depth), pyrite occurs as fine grains (~ 10 μ m), forming laminae concordant with the sedimentary bedding. In the lower part of the section (> 8 m depth), pyrite is coarser (> 100 μ m), and pyrite nodules are abundant. The similarity in $\delta^{34}S$ between nodular pyrite and laminae pyrite in the same rock chip suggests that pyrite nodules in lower sections were formed by local concentration of surrounding syndepositional fine-grained pyrite laminae [28].

Deep-water marine samples collected for analysis included six pyritic shale samples of the Jeerinah Formation (spanning 683.2–735.7 m depths) from the WRL1 core. In addition, three pyritic

shale samples (263.2, 290.6, and 311.6 m) and one dolomite (299.2 m) from the Jeerinah Formation of the RHDH2a core were analyzed. Carawine Dolomite samples from the RHDH2a core include three dolomite (161.7, 196.7, and 205.2 m) and one shale (160.6 m) samples. The two lower RHDH2a dolomite samples are granular carbonates, likely carbonate turbidite deposits, whereas the upper-most sample (161.7 m) is a laminated carbonate from a shallow-water platform facies [24]. Outcrop samples of the Jeerinah Formation near Millstream National Park have previously been studied by Kakegawa et al. [29] who reported $\delta^{34}\text{S}$ values ranging from +0.4 to +10.2‰. Values of $\delta^{34}\text{S}$ between +4.6‰ and +20.9‰ have been reported from the Carawine Dolomite succession of the same core [30].

4. Methods

4.1. Sulfur isotope analyses

Sulfur was extracted from ~ 0.5 g of powdered samples using a Kiba method [31] for the Mt. McRae Shale, and a sequential chemical extraction method [32] for the Jeerinah Formation. All extractions were undertaken at the Astrobiology Research Center at the Pennsylvania State University. The Kiba solution (tin(II) phosphate) is a strong reducing reagent that extracts both sulfate and sulfide as H_2S . Evolved H_2S is carried in a flow of nitrogen and trapped in a zinc acetate solution as zinc sulfide. The zinc sulfide is converted to silver sulfide by a silver nitrate solution. The precipitates were boiled for over 5 min; then they were collected by centrifugation and washed several times with ammonium hydroxide and deionized–distilled water. The sequential extraction method treats samples with 6 N HCl and chromium chloride [33]. This extracts acid volatile sulfur (AVS) and pyrite sulfur, respectively, as H_2S , which is then converted to silver sulfide in the same way as before. The sample was then filtered, and the solid residual was treated by Eschka fusion, precipitating the sulfur as barium sulfate. Barium sulfate was reduced by the method of Hulston and Thode [3], and converted to silver

sulfide. The isotopic composition determined by chemical separation should be treated as preliminary because of incomplete separation of AVS and pyrite sulfur [34]. Incomplete separation of pyrite sulfur and organic sulfur is also possible. Therefore, the sulfur fraction recovered by Eschka fusion is called Eschka sulfur instead of organic sulfur in the paper. Pyrite nodules and aggregates were separated and collected from dolomite samples from the core RHDH2a by digestion of rock samples by HF and HCl. The pyrite was washed with deionized water and used for fluorination.

The fluorination and isotope ratio analyses procedure is described in [10]. The prepared silver sulfide (5–5.5 mg) or pyrite grains (1.2–1.4 mg) were heated by a CO_2 laser in a F_2 atmosphere (~ 30 Torr F_2) to produce SF_6 . The product SF_6 was purified by gas chromatography and introduced into a Finnigan MAT-251 mass spectrometer to measure the abundances of $^{32}\text{SF}_5^+$, $^{33}\text{SF}_5^+$ and $^{34}\text{SF}_5^+$. This work was undertaken at the Geophysical Laboratory, Carnegie Institution of Washington.

Sulfur isotopic ratios are represented by conventional delta notation with respect to CDT as: $\delta^x\text{S} = [({}^x\text{S}/{}^{32}\text{S})_{\text{sample}}/({}^x\text{S}/{}^{32}\text{S})_{\text{CDT}} - 1] \times 1000$, where x is either 33 or 34. $\Delta^{33}\text{S}$ is a measure of deviation from mass-dependent relationship, and defined as:

$$\Delta^{33}\text{S} = 1000 \cdot \ln(1 + \delta^{33}\text{S}/1000) -$$

$$0.515 \times 1000 \cdot \ln(1 + \delta^{34}\text{S}/1000)$$

following the formulation in [4]. The $\Delta^{33}\text{S}$ calculated by this logarithmic formula was found to be the most accurate in comparing the relationship among multiple data points (see Appendix). The precision and accuracy of the fluorination system were evaluated by Hu et al. [10]. The precision is $\pm 0.2\%$ (1σ) for $\delta^{34}\text{S}$; analyses of over 100 samples of Phanerozoic sulfide samples yield $\Delta^{33}\text{S}$ values of $-0.03 \pm 0.07\%$. Ten analyses of Kiba-extracted sulfur from rocks of Phanerozoic age by the author yield $\Delta^{33}\text{S}$ of $+0.03 \pm 0.05\%$ ($\delta^{34}\text{S}$ ranging from +21 to -23%).

4.2. Photochemical model

A photochemical model of the Archean atmo-

sphere developed by Pavlov and Kasting [15] was used to compute the fluxes of atmospheric sulfur species deposited from the atmosphere as well as their isotopic systematics. The model includes 72 chemical species, which participate in 337 reactions. A separate subroutine computes sulfur isotopic photochemistry. We have assumed that the abundance of minor sulfur isotopes (^{33}S and ^{34}S) does not affect the concentration of atmospheric sulfur species. Therefore, it is legitimate to decouple the sulfur isotopic species from the rest of the model. Note that although all sulfur-involving chemical reactions have been duplicated for isotopic species, some rate constants of reactions had to be modified following the combinatorial rules described by Pavlov and Kasting [15]. In our simulations, we kept the atmospheric H_2 mixing ratio fixed at 1/20th that of CH_4 , consistent with biological control by methanogenic bacteria [35]. The atmospheric CO_2 mixing ratio was fixed at 2500 ppm. When combined with CH_4 mixing ratios of 10^{-5} to 10^{-3} , this produces mean surface temperatures between 275 K and 290 K [36], not too far from today's value of 288 K. Arguments in favor of high CH_4 concentrations in the Archean atmosphere have been published by Pavlov et al. [36,37].

Ideally, the model should keep track of different sulfur isotopes from the moment they enter the Archean atmosphere (from volcanic emission), during atmospheric fractionation, and to the moment when those sulfur isotopes are deposited on the surface in some mineralogical form. However, we cannot solve this problem self-consistently without sufficient experimental data on sulfur isotope fractionation factors (both mass-independent and mass-dependent) between species participating in photochemical reactions. Nevertheless, we can address the following problem: 'Suppose some degree of MIF ($\Delta^{33}\text{S}$) was produced in the atmosphere through some specific photochemical reactions. What MIF values can be expected in sulfur-bearing species upon deposition?'

Parameterization of the 'initial' MIF in the atmosphere has been implemented using Pavlov and Kasting's [15] approach. Following Farquhar et al. [13], we assumed that MIF is only occurring during photolysis of SO_2 ($\text{SO}_2+h\nu\rightarrow\text{SO}$) and SO

($\text{SO}+h\nu\rightarrow\text{S}+\text{O}$). Those two photolysis reactions introduce MIF into products (SO and S) and residual SO_2 and SO pools. The MIF signatures are transferred to other atmospheric sulfur through atmospheric reactions before deposition, spreading MIF between other sulfur-bearing species, diluting and partially cancelling the degree of MIF. Farquhar et al. [13,38] irradiated SO_2 (and SO_2 mixtures) with different UV sources – ArF and KrF excimer lasers, xenon and mercury lamps. They showed that for different UV sources sulfur isotopes (^{32}S , ^{33}S , ^{34}S) in the 'final' products of reactions follow different fractionation laws. Note that the 'final' products are results of multiple reactions in the reaction chamber. Neither of Farquhar's experiments was designed to measure the isotopic fractionation for individual reactions including photolysis of SO_2 (and/or SO) only.

We decided to use the fractionation dependence ($\delta^{33}\text{S}\approx 0.649\times\delta^{34}\text{S}$) from Farquhar's experiment where the UV light source resembles the continuum spectrum of solar radiation (high-pressure xenon arc lamp; continuum > 220 nm) [13,38]. Note that the chosen fractionation dependence is not able to reproduce the relationship between $\delta^{34}\text{S}$ and $\Delta^{33}\text{S}$ in our Archean data. Additional experimental data on photochemical reactions resulting in both mass-dependent and mass-independent sulfur isotope fractionation will be needed to advance beyond the present level of simplifying assumptions.

The magnitude of the 'initial' fractionation during SO_2 or SO photolysis is unknown and it is probably a function of the UV exposure time. However, no data on time of exposure are available (J. Farquhar, personal communication, 2002). Therefore, we made a number of sensitivity runs varying $\delta^{34}\text{S}$ of SO_2 and SO from -100% to -10% . We found that the magnitude of fractionation in the product is proportional to the magnitude of fractionation assigned for the two photolysis reactions. The relative size of the fractionation between SO_2 and SO photolysis reactions controls the distribution of $\Delta^{33}\text{S}$ in the products. The simulation assigning MIF only in the SO_2 photolysis produces negative $\Delta^{33}\text{S}$ for SO_2 balanced by positive $\Delta^{33}\text{S}$ for all the rest of sulfur species (S_8 , H_2SO_4 , and H_2S). Thus, both H_2SO_4

and S_8 yield positive $\Delta^{33}S$. It was found that a large fractionation during SO photolysis is necessary to produce opposite signs of $\Delta^{33}S$ for S_8 and H_2SO_4 .

Once the assumptions regarding fractionation dependence and the magnitude of fractionations were made, we implemented the fractionation of sulfur isotopes in our photochemical model by adjusting the relative photolysis rates of ^{33}SO , $^{33}SO_2$, ^{34}SO , and $^{34}SO_2$. For example, if during SO_2 photolysis the residual SO_2 has the value of $\delta^{34}S = -10\text{‰}$, then the photolysis rates have to be adjusted as $J(^{34}SO_2) = J(^{32}SO_2)/0.99$. Also, following a $\delta^{33}S \approx 0.649 \times \delta^{34}S$ fractionation law, $-J(^{33}SO_2) = J(^{32}SO_2)/0.99351$. Note that Pavlov and Kasting [15] made a mistake in assuming $J(^{34}SO_2) = 0.99 \times J(^{32}SO_2)$ (page 34). Therefore, a correction also should be made to their figure 3 (page 35): the dashed line should be reversed (SO_2 and H_2SO_4 should be below the mass fractiona-

tion line while H_2S , HS , S , SO should be above it).

5. Results

The most highly stratigraphically resolved sulfur isotope measurements were obtained from a 22-m drill core of Mt. McRae Shale from Mt. Whaleback, Newman, Australia. These samples show a trend from large positive $\Delta^{33}S$ (+6.9‰) at the 18.8-m level of the section to negative $\Delta^{33}S$ (-1.9‰) at the 2-m level of the core (Fig. 2, Table 1). Remarkably, these data exceed the range of $\Delta^{33}S$ compositions reported in [2,11] for a wide variety of Archean and early Proterozoic samples. Values of $\delta^{34}S$ and $\delta^{33}S$ show a similar trend from positive to negative, with $\delta^{34}S$ varying from +8.4 to -5.4‰. The isotopic range and stratigraphic profile of $\delta^{34}S$ reported here are con-

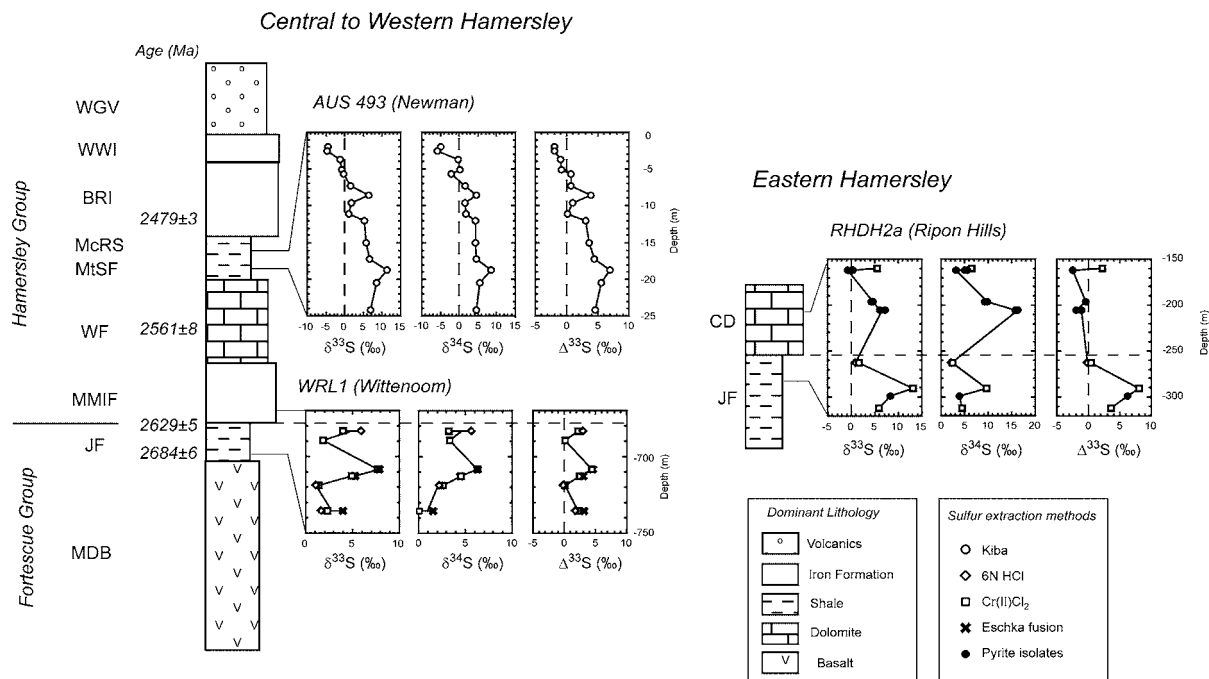


Fig. 2. Stratigraphic records of multi-S isotopes in shale and carbonate lithofacies in the late Archean Hamersley Basin, Western Australia. General stratigraphy is based on [19–21]. Ages are from U–Pb zircon data from [20,25,27]. WGV: Woongarra Volcanics, WWI: Weeli Wollli Iron Formation, BRI: Brockman Iron Formation, McRS: Mt. McRae Shale, MtSF: Mt. Sylvia Formation, WF: Wittenoom Formation, JF: Jeerinah Formation, MDB: Maddina Basalt, CD: Carawine Dolomite.

Table 1
Sulfur isotopic compositions of sulfur extracts and pyrite separates from the Hamersley Basin Australia

Depth	Method ^a	Lithology ^b	S	$\delta^{33}\text{S}$	$\delta^{34}\text{S}$	$\Delta^{33}\text{S}$
			(wt %)	(‰)	(‰)	(‰)
<i>Aus No. 493 Mt. McRae Formation</i>						
–2.0	K	S	3.1	–4.49	–5.00	–1.92
–2.6	K	S	4.1	–4.72	–5.72	–1.93
–3.7	K	S	1.6	–1.2	–0.31	–1.04
–5.1	K	S	3.1	–0.65	0.25	–0.78
–5.7	K	S	0.2	–0.38	–2.12	0.71
–7.3	K	S	1.0	1.54	1.58	0.73
–8.6	K	C	0.7	6.35	4.69	3.94
–9.6	K	S	0.7	1.81	1.55	1.01
–11.1	K	S	1.1	1.16	1.90	0.18
–12.0	K	S	3.7	5.33	4.29	3.12
–15.1	K	S	0.4	5.84	4.31	3.62
–17.2	K	S	4.5	6.73	4.54	4.39
–18.8	K	S	0.8	11.27	8.44	6.92
–20.5	K	S	0.3	8.42	5.60	5.54
–24.2	K	S	0.3	6.89	4.51	4.57
<i>WRL1 Jeerinah Formation</i>						
–683.2	C	S	2.4	3.94	3.23	2.27
–683.2	A	S	0.7	5.93	5.66	3.01
–689.6	C	S	1.8	1.83	3.34	0.12
–708.5	C	S	2.0	7.65	6.25	4.43
–708.5	E	S	0.8	7.91	6.33	4.65
–712.6	E	S	0.8	5.26	4.42	2.99
–712.6	C	S	2.3	4.91	4.57	2.56
–719.0	C	S	0.8	1.4	2.59	0.07
–719.0	A	S	0.3	1.07	2.24	–0.08
–735.7	E	S	0.1	4.01	1.53	3.22
–735.7	A	S	0.2	1.66	–0.4	1.86
–735.7	C	S	0.7	2.32	0.12	2.26
<i>RHDH2a Carawine Dolomite and Jeerinah Shale</i>						
–160.6	C	S	3.1	5.53	6.52	2.17
–161.7	P	D		0.12	5.08	–2.49
–161.7	P	D		0.37	5.48	–2.44
–161.7	P	D		–0.81	3.2	–2.45
–196.7	P	D		4.67	9.84	–0.38
–196.7	P	D		4.31	9.33	–0.48
–196.7	P	D		4.57	9.82	–0.48
–205.2	P	D		6.13	15.8	–1.97
–205.2	P	D		7.26	16.21	–1.05
–263.2	A	S	1.7	1.01	2.2	–0.13
–263.2	C	S	3.2	1.58	2.37	0.36
–290.6	C	S	0.5	13.18	9.71	8.12
–299.2	P	D		8.27	3.96	6.2
–311.6	C	S	4.6	5.88	4.47	3.57

^a A: acid volatile sulfur, C: pyrite sulfur, E: Eschka sulfur, K: Kiba sulfur, P: pyrite separate.

^b S: shale, D: dolomite, C: chert.

sistent with previous analyses by the laser-SO₂ method reported in [28].

The results on the Mt. McRae Shale have been corroborated by analyses of the 2.7 Ga Jeerinah Formation from WRL1 and RHDH2a drill cores. Samples from these cores show greater variability and are characterized by an irregular distribution of $\Delta^{33}\text{S}$ with depth. The sulfur extracted from a 53-m section of the WRL1 core yields $\Delta^{33}\text{S}$ varying from –0.1 to +4.7‰ (Fig. 2). The largest positive value was measured in the Jeerinah Formation of core RHDH2a, which yields $\Delta^{33}\text{S}$ from –0.1 to +8.1‰ (Fig. 2). The most negative value of $\Delta^{33}\text{S}$ (–2.5‰) was measured from the Carawine Dolomite, which overlies the Jeerinah Formation in core RHDH2a (Fig. 2). The values of $\delta^{34}\text{S}$ and $\Delta^{33}\text{S}$ generally correlate in the Jeerinah Formation, and are characterized by large positive $\Delta^{33}\text{S}$ (Fig. 2). In contrast, samples from the Carawine Dolomite yield negative $\Delta^{33}\text{S}$, excluding one shale sample (160.6 m).

A slight difference in both $\delta^{34}\text{S}$ and $\Delta^{33}\text{S}$ is found between sequentially extracted sulfur samples, showing some heterogeneity among different forms of sulfur in the sediments. The largest variation among extracts is detected in sample WRL1-735.7: this yields $\Delta^{33}\text{S}$ values of +1.9, +2.3 and +3.2‰ (and $\delta^{34}\text{S}$ of –0.4, 0.12, and 1.53‰) for AVS, pyrite sulfur, and Eschka sulfur, respectively (Table 1). Variations of up to 7‰ in $\delta^{34}\text{S}$ were reported from pyrite spaced along a 5-mm traverse in a single sedimentary bed in the sample from the Mt. McRae Shale [28]. Our measurements are not sensitive to spatial (mm scale) isotopic heterogeneity, however, because of the method of bulk sulfur extraction that was used. The reported heterogeneity among different sulfur extracts suggests $\Delta^{33}\text{S}$ may also be spatially heterogeneous.

6. Discussion

6.1. Production and preservation of MIF signatures

UV radiation is known to induce MIF in both oxygen and sulfur gas phase reactions [1,13].

Although several other mechanisms are known to produce MIF in oxygen or sulfur isotope systems, photochemical reaction is the only one known to produce MIF in both ^{33}S and ^{36}S [2,13]. An extraterrestrial origin of MIF is doubtful because the magnitude of the Archean anomaly is significantly larger than those reported for all classes of meteorites [38–41]. No MIF signatures have been found from over 100 analyses of sulfide and sulfate in younger rocks (> 2.0 Ga), including metamorphic rocks, hydrothermal and biogenic sulfides ($\Delta^{33}\text{S} < \pm 0.1\text{‰}$), confirming the previous reports that metamorphic, hydrothermal, and biological processes are unlikely to cause MIF [2,10].

Sulfur isotope MIF have been reported recently in sulfate aerosols collected from the atmosphere [16], and from Antarctic ice cores [18]. Analyses of ice core sulfate aerosols from two eruptive clouds that ascended into the stratosphere give $\Delta^{33}\text{S} = +0.66\text{‰}$ (Mt. Pinatubo, Philippines, 1991; Savarino, corrected value, personal communication, 2002) and $\Delta^{33}\text{S} = -0.5\text{‰}$ (eruption 1259 AD, location unknown). Analysis of sulfate aerosols from an eruptive cloud that did not reach beyond the troposphere, however, gives $\Delta^{33}\text{S} = +0.0\text{‰}$ (Cerro Hudson eruption, 1991; [18]). Analyses of sulfate aerosols sampled both above and below volcanic horizons in the ice cores show no anomalous sulfur isotope fractionation. These observations demonstrate that atmospheric reaction is capable of producing MIF in sulfur isotopes and that anomalous fractionations can be deposited on Earth's surface. The crucial role of aerosols in preserving MIF is evident. It may be asked, however, whether the discovery of mass-independent sulfur isotope fractionation in the modern atmosphere weakens the argument that the presence of Archean anomalies requires an anoxic atmosphere. The widespread prevalence of MIF in sulfur isotopes in Archean sediments is in strong contrast to its limited distribution today. The distribution of $\Delta^{33}\text{S}$ values in ice cores is zero except for events in which an eruptive cloud reached the stratosphere where it was exposed to UV light. In contrast, analyses of drill cores of black shale from Australia and South Africa [8] over an age range of 2.5–2.7 Ga, show a continuous geologic record of atmospheric production

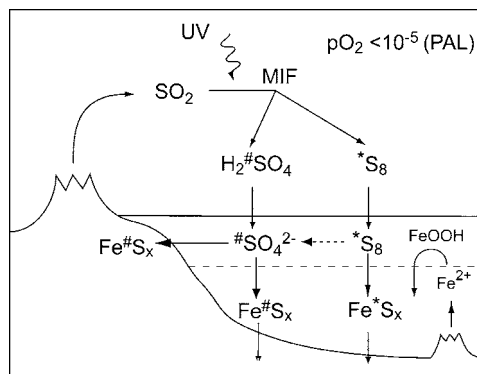


Fig. 3. A conceptual model of Archean sulfur cycle. Photochemistry in the atmosphere causes MIF in sulfur isotopes, and aerosols of S_8 and H_2SO_4 carry sulfur with positive ($^*\text{S}$) and negative ($\# \text{S}$) $\Delta^{33}\text{S}$ signatures, respectively. The preservation of MIF signatures in the sediments implies incomplete oxidation of S_8 in the ocean (dashed arrow).

of MIF sulfur as modified by microbial activity during deposition and diagenesis. The disparity in stratigraphic distribution between the present day and Archean sediments demonstrates a modern, episodic vs. an ancient, continuous production and preservation of MIF sulfur. These relationships suggest a profound difference between the modern and Archean sulfur cycle.

An anoxic Archean atmosphere is a favorable condition for both production and preservation of MIF signatures. In an Archean anoxic atmosphere, solar UV radiation was unimpeded by ozone, producing MIF in sulfur isotope systems via photolysis of SO_2 [2,13]. As pointed out by Pavlov and Kasting [15] the preservation of MIF requires more than one chemical pathway to transport atmospheric sulfur into the hydrosphere. In the absence of chemically distinct pathways, MIF signatures are erased by mixing in the atmosphere. A model atmosphere with $< 10^{-5}$ PAL oxygen is needed to produce a variety of sulfur-bearing species having different chemical behaviors [15]. This low oxygen atmospheric concentration is consistent with previous estimates based on a variety of geochemical and geological observations [42–45] (see [46,47] for an alternative idea). Actual model-predicted ground-level O_2 concentrations for the late Archean are on the order of 10^{-13} PAL [15,36,45].

In following sections, we will discuss a conceptual model for the Archean sulfur cycle. Here, an atmospheric MIF signature is transported by two chemically distinct aerosols: H_2SO_4 ($\Delta^{33}\text{S} < 0$) and S_8 ($\Delta^{33}\text{S} > 0$). Both aerosols rained out into the hydrosphere and became parts of the oceanic sulfate and S_8 reservoirs (Fig. 3). It may be seen that the preservation argument of [14,15] also applies to processes in the hydrosphere: if all S_8 was oxidized to sulfate in the ocean, the S_8 reservoir would be incorporated into the sulfate reservoir and MIF signatures erased. Therefore, preservation of a S_8 signature is favored in a low O_2 and Fe^{2+} -rich Archean ocean where at least some of S_8 precipitates as pyrite rather than being oxidized into sulfate (Fig. 3).

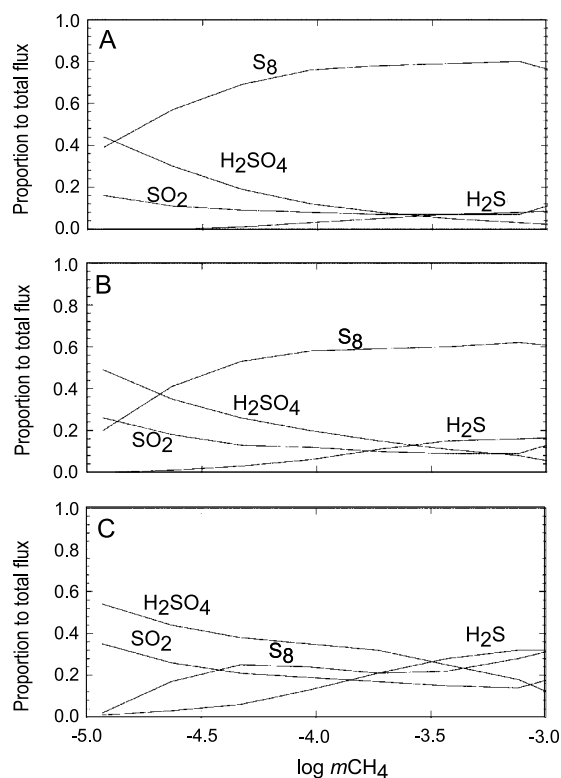


Fig. 4. Proportion of atmospheric sulfur species deposited from a model Archean atmosphere as functions of total volcanic sulfur outgassing rates and atmospheric CH_4 concentrations. Three different SO_2 outgassing rates are shown: (A) 3.5×10^9 , (B) 1×10^9 , and (C) 3.5×10^8 $\text{cm}^{-2} \text{s}^{-1}$, respectively. CO_2 mixing ratio of 2500 ppmv was used for the calculation.

6.2. Sulfur photochemistry in the Archean atmosphere

We have subjected our conceptual model to numerical testing. The numerical experiment tests whether there are atmospheric compositions capable of producing two or more mass-independently fractionated sulfur species under the conditions of solar UV-driven photochemistry.

In our model Archean atmosphere, the major sulfur-bearing species are the gases H_2S and SO_2 , and aerosols of S_8 and H_2SO_4 (Fig. 4). The elemental sulfur in the atmosphere is expected to form stable S_8 molecules and perhaps other sulfur polytropes, similar to those suggested in cloud formation on Venus [48]. The atmospheric CH_4 mixing ratio controls the overall ratio of reduced sulfur gases to oxidized ones. High CH_4 favors H_2S ; low CH_4 favors SO_2 and H_2SO_4 (Fig. 4). Elemental sulfur, S_8 , comprises a major fraction of atmospheric sulfur deposition except for a model atmosphere with highest CH_4 mixing ratio (10^{-3}) and lowest volcanic outgassing rate (Fig. 4).

A key question in interpreting our measurements concerns the source of the high $\Delta^{33}\text{S}$ values observed in the data. The laboratory measurements of Farquhar et al. [13] suggest that this signal originates from elemental sulfur (particulate S_8 in our model). The production of S_8 par-

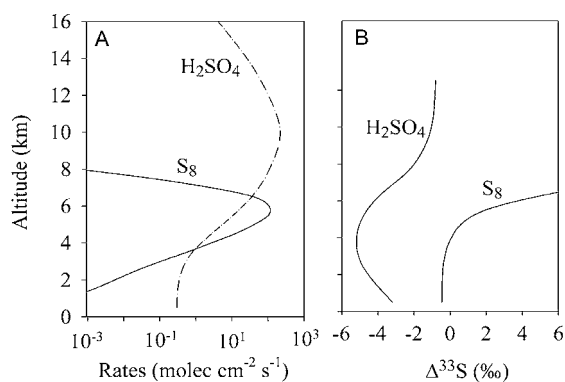


Fig. 5. Model results showing (A) formation rates of S_8 and H_2SO_4 with altitude, (B) variation of $\Delta^{33}\text{S}$ with altitude for the major sulfur species. Fractionation factors were assigned for $\delta^{34}\text{S}$ of -100 , and -20 ‰ for SO , and SO_2 photolysis reactions, respectively.

ticles is concentrated in the middle troposphere (~ 6 km altitude) in our model (Fig. 5). As this is where most of the primary sulfur photochemistry occurs, the calculated $\Delta^{33}\text{S}$ values of atmospheric species are large at this altitude (Fig. 5). If sulfur-bearing species with MIF remain in the gas phase, the MIF signature is likely to be erased by isotope exchange between the molecules. Thus, the magnitudes of MIF in gaseous species (H_2S or HS) are smaller than that of S_8 upon deposition (Fig. 6). The formation of aerosol particles, however, inhibits gas phase reactions and favors preservation of MIF signatures. Therefore, both S_8 and H_2SO_4 aerosols are deemed good carriers of atmospheric MIF signatures. They are expected to rainout into the hydrosphere, each carrying distinctive sulfur isotope compositions.

We found the fraction of S_8 in total atmospheric sulfur deposition is a strong function of total sulfur outgassing rate (Fig. 4). Estimates of modern volcanic sulfur flux vary by a factor of 10, and are on the order of $1 \times 10^9 \text{ SO}_2 \text{ molecules cm}^{-2} \text{ s}^{-1}$, or $18 \text{ Mt SO}_2 \text{ yr}^{-1}$ [49–52]. About one third of the modern flux is from explosive volcanoes and the rest is from non-explosive volcanoes [51]. At a CH_4 mixing ratio of 10^{-4} , the production of S_8 comprises $\sim 60\%$ of total sulfur removal when a sulfur outgassing rate of $1 \times 10^9 \text{ SO}_2 \text{ molecules cm}^{-2} \text{ s}^{-1}$ is used. The S_8 fraction decreases to 25% at a total sulfur flux of 3.5×10^8 and increases to 80% at a sulfur outgassing rate of $3.5 \times 10^9 \text{ molecules cm}^{-2} \text{ s}^{-1}$ (Fig. 4). The dependence of S_8 production rate on sulfur outgassing rate is intuitive, as the sequence that forms S_8 in the model contains three reactions having quadratic dependence on sulfur abundance:



Here, ‘M’ represents a third molecule necessary to carry off the excess kinetic energy of the reacting molecules. The actual reaction pathways involved in forming elemental sulfur particles are probably more complicated than assumed here. They may involve chain and ring sulfur molecules of inter-

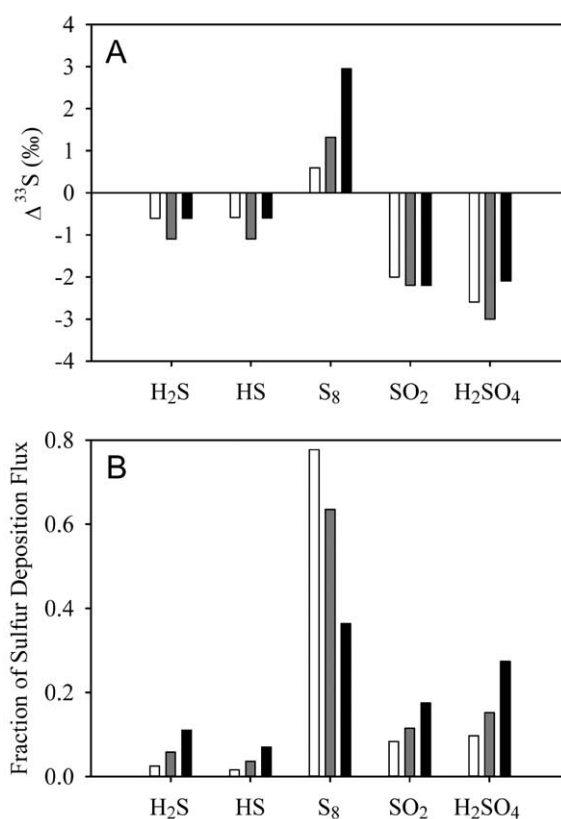


Fig. 6. Model results showing $\Delta^{33}\text{S}$ (A) and the fluxes (B) of sulfur species deposited as a function of sulfur outgassing rate. Fractionation factors used in the calculation are the same as Fig. 5. The blank, gray and filled bars represent simulations with total outgassing rates of 3.5×10^9 , 1×10^9 and $3.5 \times 10^8 \text{ molecules cm}^{-2} \text{ s}^{-1}$, respectively. CH_4 mixing ratio at 10^{-4} .

mediate lengths, e.g. S_3 , S_5 , and S_7 , as well as sulfane molecules (H_2S_n). S_8 itself is a ring molecule that represents the stable allotrope of sulfur at normal surface temperatures. Forming such a molecule must involve reactions that depend strongly on the total abundance of sulfur gases, regardless of the detailed mechanism involved.

A second result that comes out of the modeling is that the $\Delta^{33}\text{S}$ values in the S_8 particles are inversely correlated with the S_8 production rate (Fig. 6). If the production rate of S_8 is small, the average $\Delta^{33}\text{S}$ value of the removed S_8 particles is large. Conversely, if the production rate of S_8 is large, the average $\Delta^{33}\text{S}$ value of the removed S_8 particles is small. This latter result is a simple

consequence of mass balance: if most of the out-gassed SO_2 is ultimately removed as S_8 , then the average isotopic composition of the S_8 must match that of the SO_2 . The rate of Archean SO_2 outgassing could have a substantial influence on the redox balance of the Archean atmosphere [53]. The highly sensitive nature of the dependence of $\Delta^{33}\text{S}$ on SO_2 outgassing rate, in the future, may provide some constraints on the Archean volcanic SO_2 emission rate. However, such a quantitative model must await the calibration of sulfur isotope fractionation factors by laboratory experiments on photochemical reactions.

6.3. Multi-S isotope systematics in the late Archean sedimentary rocks

Today, the major source of seawater sulfate is riverine sulfate input, which comprises $\sim 90\%$ of total sulfur input into the ocean, and only 10% is from atmospheric deposition [50,52]. Under an Archean low-oxygen atmosphere, riverine input would become negligible because continental sulfide minerals would not have been oxidized during weathering. Thus, atmospheric deposition of sulfuric acid could have been a dominant source for the seawater sulfate [2,13,50].

We suggest that Archean atmospheric photochemical reactions partitioned sulfur isotopes such that H_2SO_4 had negative values for $\delta^{34}\text{S}$ and $\Delta^{33}\text{S}$, with S_8 positive in $\Delta^{33}\text{S}$ and $\delta^{34}\text{S}$ (Fig. 7A). It is expected that atmospheric sulfur isotope fractionations would have been modified by microbial metabolism. Bacterial sulfate reduction could have operated as early as 3.4 Ga [54,55]. The bacterial sulfate reduction and subsequent precipitation of sedimentary pyrite could have been the main sink for seawater sulfate by the late Archean. Sulfate reducing bacteria are known to produce fractionations in $\delta^{34}\text{S}$ of up to $\sim 50\%$ with respect to sulfate [56,57]. Thus, bacterial reduction of seawater sulfate produces sulfide depleted in ^{34}S such that remaining sulfate becomes enriched in ^{34}S (Fig. 7A). Because the isotope fractionation is mass-dependent [58], $\Delta^{33}\text{S}$ of seawater sulfate remains negative.

Our best estimate of the sulfur isotopic composition of Archean seawater sulfate is $\sim -2\%$ for

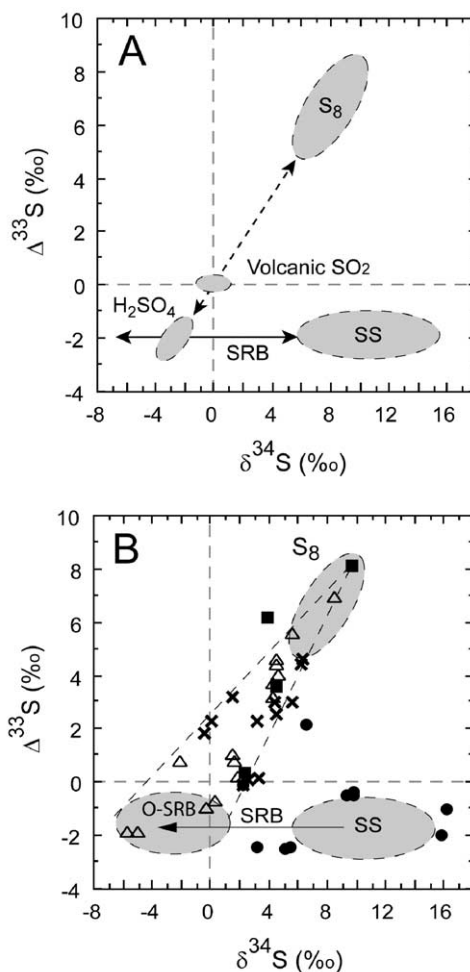
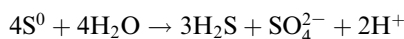


Fig. 7. Multiple sulfur isotope systematics for the late Archean sediments in the Hamersley Basin. (A) Atmospheric MIF and mass-dependent fractionation by sulfate reducing bacteria (SRB) is shown in dashed and solid arrows, respectively. Gray fields represent isotopic composition of volcanic SO_2 , S_8 and H_2SO_4 aerosols, and seawater sulfate (SS). (B) Similar to (A) but isotope data are plotted. Filled square: Jeerinah Formation (RHDH2a), x: Jeerinah Formation (WRL1), open triangle: Mt. McRae Shale, filled circle: Carawine Dolomite. The field O-SRB represents estimated field of pyrite formed by bacterial sulfate reduction in a pelagic environment.

$\Delta^{33}\text{S}$ and $+6$ to $+16\%$ for $\delta^{34}\text{S}$ (Fig. 7A,B). The assignment of negative $\Delta^{33}\text{S}$ for oceanic sulfate is consistent with negative values of $\Delta^{33}\text{S}$ measured in sulfate sulfur from ~ 3.4 Ga Archean barite deposits in both South Africa and Australia [2]

and in sulfide sulfur from 2.7 Ga volcanogenic massive sulfide deposits [9]. Because dissolved seawater sulfate is an important source of sulfur in both types of deposits their negative $\Delta^{33}\text{S}$ indicates that seawater sulfate had a negative value of $\Delta^{33}\text{S}$. Our estimate of $\delta^{34}\text{S}$ is consistent with previous estimates based on a small number of data on Archean sedimentary sulfate minerals [59].

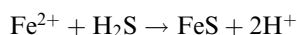
The fate of S_8 after deposition into the hydrosphere is unclear. Elemental sulfur is thermodynamically unstable in an aqueous phase, where it disproportionates to sulfide and sulfate:



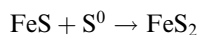
This either occurs inorganically or mediated by bacteria. In a low temperature system ($< 200^\circ\text{C}$), inorganic disproportionation involves only a minor ($< 3\%$) kinetic isotope fractionation [60]. Biologically mediated disproportionation produces H_2S depleted in ^{34}S by $\sim 7\%$ [57,61].

Microbes utilize S^0 (and a variety of intermediate sulfur species) as both electron donor and acceptor. The reduction of S^0 to H_2S uses H_2 or organic compounds as electron donors [59]. The oxidation of S^0 to sulfate may be mediated by sulfur-oxidizing bacteria, by using NO_3^- or O_2 as electron acceptors, or phototrophic sulfur bacteria [57,62]. Microbial oxidation and reduction of S^0 produces only minor fractionation of S isotopes [57,63].

Microbial processes involving intermediate sulfur species are unlikely to induce MIF [58]. Thus, oxidation of S^0 to sulfate would not change $\Delta^{33}\text{S}$ of the remaining S^0 reservoir but the addition of positive $\Delta^{33}\text{S}$ in S_8 to the negative $\Delta^{33}\text{S}$ seawater sulfate reservoirs would increase the sulfate reservoirs $\Delta^{33}\text{S}$ composition. As discussed earlier, if all the S_8 is oxidized to sulfate, the MIF signature will be erased in the ocean. Thus, at least some fraction of S^0 should have precipitated as pyrite (or other sulfide minerals) before it was oxidized to sulfate. Note that precipitation of pyrite can be written as:



and:



where the latter reaction proceeds via polysulfide or other metastable intermediates [64–66]. Thus, some of the sulfur in pyrite could have been derived from sulfide and some from S^0 .

The large variation of $\delta^{34}\text{S}$ (+3.2 to +16.2‰) and negative $\Delta^{33}\text{S}$ (−2.5 to −0.4) of pyrite sulfur in the Carawine Dolomite is attributed to bacterial reduction of seawater sulfate because this process is expected to produce pyrite with variable $\delta^{34}\text{S}$ and negative $\Delta^{33}\text{S}$ inherited from seawater sulfate (Fig. 7B). The relatively high $\delta^{34}\text{S}$ indicates sulfate reduction in a closed system with respect to seawater sulfate [67]. Active biological activity in the Carawine platform could have sustained a relatively fast sulfate reduction rate either in the water column or at the sediment–water interface. Because of the low sulfate supply rate into the ocean, the sulfate reduction rate would have exceeded the supply rate of sulfate. The isotopic composition of sulfide produced in such a closed system would become identical to the isotopic composition of seawater sulfate.

The data from the Mt. McRae Shale and the Jeerinah Formation are characterized by a large positive $\Delta^{33}\text{S}$ of up to +8.1‰. The $\Delta^{33}\text{S}$ is roughly correlated to $\delta^{34}\text{S}$ ($\Delta^{33}\text{S} \approx 0.51 + 0.64 \times \delta^{34}\text{S}$; $R^2 = 0.69$) (Fig. 7B). This relationship between $\delta^{34}\text{S}$ and $\Delta^{33}\text{S}$ is observed for both formations, despite the fact that each core shows irregular variations in $\Delta^{33}\text{S}$ profile, despite a disparity in age of ~ 200 Ma, and despite a geographical separation of over 300 km. The $\delta^{34}\text{S}$ – $\Delta^{33}\text{S}$ relationship in shale is explained by mixing two sources of sulfur in pyrite: one component is derived from sulfide from bacterial sulfate reduction (with negative and variable $\delta^{34}\text{S}$; O-SRB in Fig. 7B) and the other one derived from S_8 (with large positive $\Delta^{33}\text{S}$) (Fig. 7B).

An isotopic fractionation of ca. 15‰ in $\delta^{34}\text{S}$ between estimated seawater sulfate (+6 to +16‰) and a sulfate-derived pyrite end-member (−6 to +1‰) (Fig. 7B, arrow SRB) is consistent with isotopic fractionation induced by sulfate reducing bacteria under low sulfate concentrations [59,68]. A sulfate level between 0.2 and 1 mM was obtained from the diagenetic model of Habicht et

al. (figure 2A in [68]). Such a low sulfate concentration is expected for the Archean sulfur cycle in which the main source of oceanic sulfate was derived from the atmosphere. This low sulfate level would have also suppressed bacterial sulfate reduction rates. Therefore, in environments where S_8 -derived pyrite was produced, the MIF signature of sulfate-derived pyrite could have been easily diluted.

Pyrite formed from S_8 would yield a large positive $\Delta^{33}S$ inherited from atmospheric S_8 . The small variation in $\delta^{34}S$ in this component (Fig. 7B) is consistent with microbial S^0 reduction (or inorganic S^0 disproportionation) rather than microbial S^0 disproportionation because the latter is known to fractionate $\delta^{34}S$. Reduction of S^0 is thought to be among the oldest of metabolisms because it is widespread in the Archea and Bacteria domains [59]. It has been suggested that early metabolic S^0 reduction was supported by a hydrothermal source of S^0 [59]. Our data suggest that microbial S^0 reduction could have been widespread in the Archean ocean supported by an atmospheric source of S_8 .

7. Conclusion

Our study compares measured sulfur isotope profiles with predictions of computer models of the Archean atmosphere to establish a working model for the origin and preservation of mass-independent sulfur isotope fractionation in Archean sediments. Because model calculations are highly dependent on the experimental simulation of MIF between sulfur-bearing gas phase species at UV wavelengths present in the solar spectrum [13], the detailed sulfur isotope systematics remain tentative despite the mutual consistency of observations, experiments, and calculations. Thus, there is a particular need for additional experiments to closely investigate the mechanisms of fractionation by photochemistry induced by UV radiation.

Our data indicate lithologic control over the systematics of three isotopes of sulfur. An appreciation of depositional environments is required to understand mechanisms for preserving their fractionations in Archean rock records. The de-

tailed documentation of Archean $\delta^{34}S$ and $\Delta^{33}S$ records both temporally and geographically will map the distribution of sulfur metabolism in the Archean Earth. Thus, investigation of multi-sulfur isotope systematics is a powerful tool to trace atmospheric, hydrospheric and biological processes in the ancient sulfur cycle. New insights are to be realized into the chemical evolution of the atmosphere and hydrosphere as well as the evolution and distribution of Archean sulfur-metabolizing organisms.

Acknowledgements

We thank H. Ohmoto, H. Naraoka, K. Yamaguchi, H. Chiba, M. Kusakabe, and Y. Watanabe for providing samples, and B. Wing, M. Bau, B. Simonson, J. Scott, L. Kump, M. Arthur, H. Bao, A. Bekker, G. Hu, and P.-L. Wang for advice and critical discussion. Reviews by J. Farquhar and R. Summons improved the manuscript and are acknowledged with gratitude. Financial support came from the NASA National Astrobiology Institute to the Carnegie Institution, the Pennsylvania State University, and the University of Colorado. Grants from the National Science Foundation, EAR-0125096, to D.R. and EAR-0073831 to K.H.F. provided additional support. Construction costs for the laser fluorination system for analysis of sulfide minerals at the Geophysical Laboratory were met by the Jet Propulsion Laboratory, contract 1213932, to P.G. Conrad, K. Nealson, M. Fogel, W. Huntress, and D.R. [KF]

Appendix. Calculation of $\Delta^{33}S$ values

We have used the formulation suggested by Miller [4] to calculate $\Delta^{33}S$ values because this formula was found to be the most accurate in expressing the relationship between multiple data points. From equation (2) in Miller [4]:

$$\left(\frac{{}^{33}R_{sa}}{{}^{33}R_{CDT}}\right) = (1 + k) \left(\frac{{}^{34}R_{sa}}{{}^{34}R_{CDT}}\right)^\lambda \quad (\text{a.1})$$

where λ represents the relationship of the mass-

dependent fractionation that depends upon the type of fractionation (equilibrium vs. kinetic etc.), and $(1+k)$ represents the offset from an isotope reference material (i.e. CDT).

Let us consider a reservoir whose isotope ratio deviates from a terrestrial fractionation line (or more precisely, CDT). The mass-independent component in the reservoir can be best represented by having non-zero value for k . If secondary processes (e.g. biological or metamorphic processes) occur in the reservoir that fractionate sulfur isotopes mass-dependently, such a process would fractionate $^{34}\text{R}_{\text{sa}}$ and $^{33}\text{R}_{\text{sa}}$ following a mass-dependent rule (i.e. $^{33}\text{R}_{\text{sa}} = ^{34}\text{R}_{\text{sa}}^\lambda$) but the value of k will be constant.

From equation (a.1):

$$\ln(1+k) = \ln\left(\frac{^{33}\text{R}_{\text{sa}}}{^{33}\text{R}_{\text{CDT}}}\right) - \lambda \ln\left(\frac{^{34}\text{R}_{\text{sa}}}{^{34}\text{R}_{\text{CDT}}}\right) \quad (\text{a.2})$$

By definition:

$$\frac{^{33}\text{R}_{\text{sa}}}{^{33}\text{R}_{\text{CDT}}} = \left(\frac{\delta^{33}\text{S}}{1000} + 1\right), \text{ and}$$

$$\frac{^{34}\text{R}_{\text{sa}}}{^{34}\text{R}_{\text{CDT}}} = \left(\frac{\delta^{34}\text{S}}{1000} + 1\right)^\lambda \quad (\text{a.3})$$

Multiplying equation (a.2) by 1000, $\Delta^{33}\text{S}$ can be defined as:

$$\Delta^{33}\text{S} \equiv 1000 \cdot \ln(1+k) =$$

$$1000 \cdot \left\{ \ln\left(\frac{\delta^{33}\text{S}}{1000} + 1\right) - \lambda \ln\left(\frac{\delta^{34}\text{S}}{1000} + 1\right) \right\} \quad (\text{a.4})$$

Here, $\Delta^{33}\text{S}$ is only a function of k , thus, the secondary mass-dependent fractionation processes would not change $\Delta^{33}\text{S}$. It is important to find a relationship among multiple data points by identifying the secondary mass-dependent fractionation processes.

From (a.1):

$$k \cdot \left(\frac{^{34}\text{R}}{^{34}\text{R}}\right)^\lambda = \left(\frac{^{33}\text{R}}{^{33}\text{R}}\right) - \left(\frac{^{34}\text{R}}{^{34}\text{R}}\right)^\lambda \quad (\text{a.5})$$

Multiplying both sides of (a.5) by 1000 gives the formula defined by Farquhar et al. [2]:

$$\Delta^{33}\text{S} \equiv 1000 \cdot k \cdot \left(\frac{\delta^{34}\text{S}}{1000} + 1\right)^\lambda =$$

$$1000 \cdot \left\{ \left(\frac{\delta^{33}\text{S}}{1000} + 1\right) - \left(\frac{\delta^{34}\text{S}}{1000} + 1\right)^\lambda \right\} \quad (\text{a.6})$$

Here, $\Delta^{33}\text{S}$ is not only a function of k but also $\delta^{34}\text{S}$. The secondary mass-dependent fractionation process would yield slightly different $\Delta^{33}\text{S}$ values when $\delta^{34}\text{S}$ deviated significantly from zero.

References

- [1] M.H. Thiemens, Mass-independent isotope effects in planetary atmospheres and the early solar system, *Science* 283 (1999) 341–345.
- [2] J. Farquhar, H. Bao, M.H. Thiemens, Atmospheric influence of Earth's earliest sulfur cycle, *Science* 289 (2000) 756–759.
- [3] J.R. Hulston, H.G. Thode, Variations in the S^{33} , S^{34} , and S^{36} contents of meteorites and their relation to chemical and nuclear effects, *J. Geophys. Res.* 70 (1965) 3475–3484.
- [4] M.F. Miller, Isotopic fractionation and the quantification of ^{17}O anomalies in the oxygen three-isotope system an appraisal and geochemical significance, *Geochim. Cosmochim. Acta* 66 (2002) 1881–1889.
- [5] Y.Q. Gao, R.A. Marcus, Strange and unconventional isotope effects in ozone formation, *Science* 293 (2001) 259–263.
- [6] K. Mauersberger, B. Erbacher, D. Krankowsky, J. Günther, R. Nickel, Ozone isotope enrichment: Isotopomer-specific rate coefficients, *Science* 283 (1999) 370–372.
- [7] J. Farquhar, H. Bao, M.H. Thiemens, G. Hu, D. Rumble, Questions regarding Precambrian sulfur isotope fractionation – Response, *Science* 292 (2001) 5524.
- [8] A. Bekker, H.D. Holland, D. Rumble, W. Yang, P.-L. Wang, L.L. Coetsee, MIF of S, oolitic ironstones, redox sensitive elements in shales, and the rise of atmospheric oxygen, *Geochim. Cosmochim. Acta* 66 (2002) A64.
- [9] B.A. Wing, J. Farquhar, D. Rumble, J.W. Valley, $\Delta^{33}\text{S}$ evidence from superior province ore deposits for a sulfate-stratified ocean at 2.7 Ga, *Abstracts with Programs* 34, *Geol. Soc. Am.*, 2002, p. 516.
- [10] G. Hu, D. Rumble, P.-L. Wang, An ultraviolet laser microprobe for the analysis of multi-sulfur isotopes and its use in measuring Archean sulfur isotope mass-independent anomalies, *Geochim. Cosmochim. Acta* (in press).
- [11] S.J. Mojzsis, C.D. Coath, J.P. Greenwood, K.D. McKeehan, T.M. Harrison, Mass-independent isotope effects in Archean (2.5 to 3.8 Ga) sedimentary sulfides determined by ion microprobe analysis, *Geochim. Cosmochim. Acta* 67 (2003) 1635–1658.

- [12] B. Runnegar, C. Coath, J.R. Lyons, K.D. Mckeegan, Mass-independent and mass-dependent sulfur processing throughout the Archean, *Geochim. Cosmochim. Acta* 66 (2002) A64.
- [13] J. Farquhar, J. Savarino, S. Airieau, M.H. Thiemens, Observation of wavelength-sensitive mass-independent sulfur isotope effects during SO₂ photolysis: Implications for the early atmosphere, *J. Geophys. Res.* 106 (2001) 1–11.
- [14] J.F. Kasting, The rise of atmospheric oxygen, *Science* 293 (2001) 819–820.
- [15] A.A. Pavlov, J.F. Kasting, Mass-independent fractionation of sulfur isotopes in Archean sediments: Strong evidence for an anoxic Archean atmosphere, *Astrobiology* 2 (2002) 27–41.
- [16] A. Romero, M.H. Thiemens, Mass-independent sulfur isotopic compositions in sulfate aerosols and surface sulfates derived from atmospheric deposition: possible sources of the MI anomaly and implications for atmospheric chemistry, *EOS Trans. AGU*, 83, Fall Meet. Suppl., 2002, B71A-0731.
- [17] H. Bao, G. Michalski, M.H. Thiemens, Sulfate oxygen-17 anomalies in desert varnishes, *Geochim. Cosmochim. Acta* 65 (2001) 2029–2036.
- [18] J. Savarino, J. Cole-Dai, S. Bekky, A. Romero, T. Jackson, Sulfur oxidation chemistry preserved in South Pole snow and ice: The origin of sulfur and oxygen mass-independent fractionations generated in plinian eruptions, *EOS Trans. AGU*, 83, Fall Meet. Suppl., 2002, B61D-11.
- [19] A.F. Trendall, J.G. Blockley, The iron formations of the Precambrian Hamersley Group, Western Australia, *Western Australia Geol. Surv. Bull.* 119, 1970, 366 pp.
- [20] N.T. Arndt, D.R. Nelson, W. Compston, A.F. Trendall, A.M. Thorne, The age of the Fortescue Group, Hamersley Basin, Western Australia, from ion microprobe zircon U–Pb results, *Aust. J. Earth Sci.* 38 (1991) 261–281.
- [21] T.S. Blake, M.E. Barley, Tectonic evolution of the late Archean to early Proterozoic Mount Bruce Megasequence set, Western Australia, *Tectonics* 11 (1992) 1415–1425.
- [22] A.M. Thorne, A.F. Trendall, Geology of the Fortescue Group, Pilbara Craton, Western Australia, *Geol. Surv. Western Australia Bull.* 144, 2001, 249 pp.
- [23] R.E. Smith, J.L. Perdrix, T.C. Parks, Burial metamorphism in the Hamersley Basin, Western Australia, *J. Petrol.* 23 (1982) 75–102.
- [24] B.M. Simonson, K.A. Schubel, S.W. Hassler, Carbonate sedimentology of the early Precambrian Hamersley Group of Western Australia, *Precambrian Res.* 60 (1993) 287–335.
- [25] D.R. Nelson, A.F. Trendall, W. Altermann, Chronological correlations between the Pilbara and Kaapvaal cratons, *Precambrian Res.* 97 (1999) 165–189.
- [26] R.C. Morris, Genetic modelling for banded iron-formation of the Hamersley Group, Pilbara Craton, Western Australia, *Precambrian Res.* 60 (1993) 243–286.
- [27] A.F. Trendall, J.R. de Laeter, D.R. Nelson, S.W. Hassler, Precise zircon U–Pb ages from the Marra Mamba Iron Formation and the Wittenoom Formation Hamersley Group Western Australia, *Austral. J. Earth Sci.* 45 (1998) 137–142.
- [28] T. Kakegawa, H. Kawai, H. Ohmoto, Origins of pyrites in the ~2.5 Ga McRae Shale, the Hamersley District, Western Australia, *Geochim. Cosmochim. Acta* 62 (1999) 3205–3220.
- [29] T. Kakegawa, Y. Kasahara, K.-I. Hayashi, H. Ohmoto, Sulfur and carbon isotope analyses of the 2.7 Ga Jeerinah Formation, Fortescue Group, Australia, *Geochim. J.* 34 (2000) 121–133.
- [30] D.J. Bottomley, J. Veizer, H. Nielsen, M. Moczydlowska, Isotopic composition of disseminated sulfur in Precambrian sedimentary rocks, *Geochim. Cosmochim. Acta* 56 (1992) 3311–3322.
- [31] A. Sakai, Y. Arikawa, R.E. Folinsbee, Kiba reagent method of sulfur extraction applied to isotopic work, *Bull. Geol. Surv. Jpn.* 30 (1979) 241–245.
- [32] M.L. Tuttle, M.B. Goldhaber, D.L. Williamson, An analytical scheme for determining forms of sulphur in oil shales and associated rocks, *Talanta* 33 (1986) 953–961.
- [33] D.E. Canfield, R. Raiswell, J.T. Westrich, C.M. Reaves, R.A. Berner, The use of chromium reduction in the analysis of reduced inorganic sulfur in sediments and shales, *Chem. Geol.* 54 (1986) 149–155.
- [34] C.A. Rice, M.L. Tuttle, R.L. Reynolds, The analysis of forms of sulfur in ancient sediments and sedimentary rocks: comments and cautions, *Chem. Geol.* 107 (1993) 83–95.
- [35] J.F. Kasting, A.A. Pavlov, J.L. Siefert, A coupled ecosystem-climate model for predicting the methane concentration in the Archean atmosphere, *Orig. Life Evol. Biosph.* 31 (2001) 271–285.
- [36] A.A. Pavlov, J.F. Kasting, L.L. Brown, K.A. Rages, R. Freedman, Greenhouse warming by CH₄ in the atmosphere of early Earth, *J. Geophys. Res.* 105 (2000) 11981–11990.
- [37] A.A. Pavlov, J.F. Kasting, J.L. Eigenbrode, K.H. Freeman, Organic haze in Earth's early atmosphere: Source of low-¹³C Late Archean kerogens?, *Geology* 29 (2001) 1003–1006.
- [38] J. Farquhar, J. Savarino, T.L. Jackson, M.H. Thiemens, Evidence of atmospheric sulphur in the Martian regolith from sulphur isotopes in meteorites, *Nature* 404 (2000) 50–52.
- [39] X. Gao, M.H. Thiemens, Systematic study of sulfur isotopic composition in iron meteorites and the occurrence of excess ³³S and ³⁶S, *Geochim. Cosmochim. Acta* 55 (1991) 2671–2679.
- [40] H.G. Rees, A. Thode, A ³³S anomaly in the Allende meteorite, *Geochim. Cosmochim. Acta* 41 (1977) 1679–1682.
- [41] J.P. Greenwood, S.J. Mojzsis, C.D. Coath, Sulfur isotopic compositions of individual sulfides in Martian meteorites ALH 84001 and Nakhla: implications for crust-regolith exchange on Mars, *Earth Planet. Sci. Lett.* 184 (2000) 23–35.
- [42] P. Cloud, A working model of the primitive Earth, *Am. J. Sci.* 272 (1972) 537–548.

- [43] H.D. Holland, *The Chemical Evolution of the Atmosphere and Oceans*, Princeton University Press, Princeton, NJ, 1984, 582 pp.
- [44] J.C.G. Walker, C. Klein, M. Schidlowski, J.W. Schopf, D.J. Stevenson, M.R. Walter, Environmental evolution of the Archean-Early Proterozoic Earth, in: J.W. Schopf (Ed.), *Earth's Earliest Biosphere*, Princeton University Press, NJ, 1983, pp. 261–290.
- [45] J.F. Kasting, Earth's early atmosphere, *Science* 259 (1993) 920–926.
- [46] H. Ohmoto, Evidence in pre-2.2 Ga paleosols for the early evolution of atmospheric oxygen and terrestrial biota, *Geology* 24 (1996) 1135–1138.
- [47] H. Ohmoto, When did the Earth's atmosphere become oxic?, *Geochem. News* 93 (1997) 13.
- [48] Y.L. Yung, W.B. DeMore, *Photochemistry of Planetary Atmospheres*, Oxford University Press, New York, 1999, 456 pp.
- [49] H. Berresheim, W. Jaeschke, The contribution of volcanoes to the global atmospheric sulfur budget, *J. Geophys. Res.* 88 (1983) 3732–3740.
- [50] J.C.G. Walker, P. Brimblecombe, Iron and sulfur in the pre-biologic ocean, *Precambrian Res.* 28 (1985) 205–222.
- [51] G.J.S. Bluth, C.C. Schnetzler, A.J. Krueger, L.S. Walter, The contribution of explosive volcanism to global atmospheric sulphur dioxide concentrations, *Nature* 366 (1993) 327–329.
- [52] M.A. Arthur, Volcanic contributions to the carbon and sulfur geochemical cycles and global change, in: R.D. Ballard (Ed.), *Encyclopedia of Volcanoes*, Academic Press, CA, 2000, pp. 1045–1056.
- [53] H.D. Holland, Volcanic gases, black smokers, and the great oxidation event, *Geochim. Cosmochim. Acta* 66 (2002) 3811–3826.
- [54] H. Ohmoto, T. Kakegawa, D. Lowe, 3.4-billion-year-old biogenic pyrite from Barberton, South Africa: sulfur isotope evidence, *Science* 262 (1993) 555–557.
- [55] Y. Shen, R. Buick, D.E. Canfield, Isotope evidence for microbial sulphate reduction in the early Archean era, *Nature* 410 (2001) 77–81.
- [56] H. Ohmoto, M.B. Goldhaber, Sulfur and carbon isotopes, in: H.L. Barnes (Ed.), *Geochemistry of Hydrothermal Ore Deposits*, John Wiley and Sons, NY, 1997, pp. 519–611.
- [57] D.E. Canfield, Biogeochemistry of sulfur isotopes, in: J.W. Valley, D.R. Cole (Eds.), *Stable Isotope Geochemistry*, *Rev. Mineral. Geochem.* 43, Mineral. Soc. Am. Washington, DC, 2001, pp. 607–636.
- [58] J. Farquhar, B. Wing, Multiple sulfur isotopes and the evolution of the atmosphere, *Earth Planet. Sci. Lett.* (in press).
- [59] D.E. Canfield, R. Raiswell, The evolution of the sulfur cycle, *Am. J. Sci.* 299 (1999) 697–723.
- [60] J.W. Smith, Isotopic fractionations accompanying sulfur hydrolysis, *Geochem. J.* 34 (2000) 95–99.
- [61] D.E. Canfield, B. Thamdrup, S. Fleisher, Isotope fractionation and sulfur metabolism by pure and enrichment cultures of elemental sulfur-disproportionating bacteria, *Limnol. Oceanogr.* 43 (1998) 253–264.
- [62] H.G. Schlegel, B. Bowien, *Autotrophic Bacteria*, FEMS symposium 42, Science Tech publications, Madison, WI, 1989, 528 pp.
- [63] B. Fry, J. Cox, H. Gest, J.M. Hays, Discrimination between ^{34}S and ^{32}S during bacterial metabolism of inorganic sulfur compounds, *J. Bacteriol.* 165 (1986) 328–330.
- [64] R.A. Berner, Sedimentary pyrite formation, *Am. J. Sci.* 268 (1970) 1–23.
- [65] D.T. Rickard, Kinetics and mechanism of pyrite formation at low temperatures, *Am. J. Sci.* 275 (1975) 636–652.
- [66] M.A.A. Schoonen, H.L. Barnes, Reactions forming pyrite and marcasite from solution; II, Via FeS precursors below 100°C, *Geochim. Cosmochim. Acta* 55 (1991) 3491–3504.
- [67] H. Ohmoto, Biogeochemistry of sulfur and the mechanisms of sulfide-sulfate mineralization in Archean oceans, in: M. Schidlowski (Ed.), *Early Organic Evolution: Implications for Mineral and Energy Sources*, Springer-Verlag, Berlin, 1992, pp. 378–397.
- [68] K.S. Habicht, M. Gade, B. Thamdrup, P. Berg, D.E. Canfield, Calibration of sulfate levels in the Archean ocean, *Science* 298 (2002) 2372–2374.